Available online at www.sciencedirect.com
SCIENCE DIRECT®
Journal of Nuclear Materials 343 (2005) 184–190
journal of nuclear materials
www.elsevier.com/locate/jnucmat

Mechanical properties and microstructure of $AlMg_3$ irradiated in SINQ Target-3

Y. Dai *, D. Hamaguchi

Spallation Neutron Source Division, Paul Scherrer Institut, 5232 Villigen PSI, Switzerland

Abstract

An aluminum alloy $AlMg_3$ has been used as the material for safety-hulls of SINQ targets. In the present work, the mechanical properties and microstructure of the material from the beam window of the safety-hull of SINQ Target-3 has been investigated. The tensile test results indicate that both yield stress and ultimate tensile strength increased significantly after irradiation. Meanwhile, for the specimens from the beam centre area irradiated to about 3.6 dpa, their ductility reduced substantially. However, these specimens broke in a ductile fracture mode. TEM observations show that the irradiation induced high-density dislocation loops and helium bubbles. The bubbles locate preferentially at dislocations and grain boundaries. The bubbles at grain boundaries are much larger than those in grain interior. The presence of high-density bubbles may enhance both irradiation hardening and embrittlement effects.

1. Introduction

Due to their high thermal conductivity, low absorption of thermal neutrons, and more important, excellent radiation damage resistance, aluminum–magnesium alloys are widely engaged in nuclear applications. In the Swiss Spallation Neutron Source (SINQ), an aluminum–magnesium alloy, $AlMg_3$ (close to Al-5454), has been used for the safety-hulls of the targets, which receive intensive irradiation damage induced by high energy protons and spallation neutrons, particularly at the proton beam entrance window [1]. Up-to-date four targets have been successfully operated in SINQ during the last seven years. For a safe operation of SINQ targets, it is of essential importance to investigate the changes in the mechanical properties and microstructure of this material after irradiation. Meanwhile, for developing new spallation sources where Al-alloys are considered as tentative beam window materials, it needs urgently the basic understanding of the behavior of these alloys in spallation radiation environments. Therefore, tensile tests and transmission electron microscopy (TEM) investigations have been performed on the safety-hull of Target-3 irradiated in 1998 and 1999. The microstructure of the material in both irradiated and unirradiated conditions has been studied and reported in detail elsewhere [2]. In the present paper, the results of the microstructure will be briefly described and the irradiation induced changes of mechanical properties will be reported and discussed based on the results of the microstructure study.

2. Experimental

The composition of the $AlMg_3$ alloy is in wt%: 2.72Mg, 0.3Si, 0.25Fe, 0.35Mn and balanced by Al.

* Corresponding author. Tel.: +41 56 310 4171; fax: +41 56 310 4529.
E-mail address: yong.dai@psi.ch (Y. Dai).

0022-3115/$ - see front matter © 2005 Elsevier B.V. All rights reserved.
doi:10.1016/j.jnucmat.2004.11.021

The original material was in form of cylinders of about 230 mm in diameter and about 150 mm long. The heat treatment was not given by the producer. However, the microstructure and the yield stress of the as-received material indicate that it should be in an annealed condition. From the cylinders, hemisphere walls of the windows were milled. As illustrated schematically in Fig. 1, the safety-hull is a double walled container of about 200 mm in diameter and about 2 m long from the bottom of the beam entrance window to the upper flange. The thickness of the walls is 4 mm in the straight part, and changes gradually from 4 mm to 2 mm at the bottom of the beam window. There is a gap of 2–3 mm (depending on the position) between the two walls. Cooling water (D_2O) of about 40 °C runs through the gap and inside to cool the hull and the target block during irradiation. The outer surface of the outer wall faces to vacuum. However, the irradiation temperature of the outer wall is only a few degrees higher than that of the inner wall with a maximum value less than 60 °C [3].

SINQ Target-3 received a total proton charge of 6.8 A h and with a peak fluence of about 3.2×10^{25} m^{-2} at the beam window of the safety-hull. The energy of the proton beam was about 570 MeV. The irradiation dose, helium and hydrogen concentrations at the peak fluence position are about 3.6 dpa, 1125 appm He and 1900 appm H, respectively [4,5]. After irradiation, discs of 40 mm in diameter were cut from the centre and edge areas of the beam footprint (Fig. 2) for post-irradiation examinations.

In order to determine the profile of the proton beam, γ-mapping was performed on the discs. Fig. 3 shows an example of the results of the disc from the centre area of the window. It can be seen that the proton beam has an elliptical profile. However, it is impossible to deduce the complete profile of the proton beam from the γ-mapping results because the size of the discs is too small. Hence, the proton fluence was still calculated from the known proton beam geometry [4].

After γ-mapping, tensile specimens with a size of 20×5 mm and a gauge area of 7×2.5 mm were cut from the discs. The tensile specimens were polished on both sides to remove the curvature, which resulted in a final thickness of about 1.4 mm. Four specimens were cut from each disc, see Fig. 4. From each of the two discs in the beam central area, two specimens were cut symmetrically to the long axis of the beam profile.

Tensile tests were performed at room temperature on a 2 kN MTS mechanical testing machine. Five irradiated specimens of doses 0.7, 2.7, 3.2 and 3.6 dpa were tested. For comparison, a few specimens were prepared in the

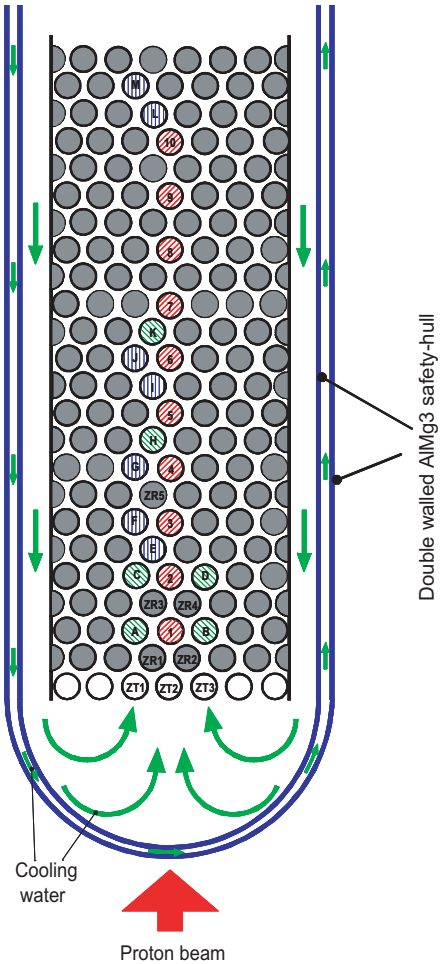

Fig. 1. A schematic sketch showing the lower part of SINQ Target-3.

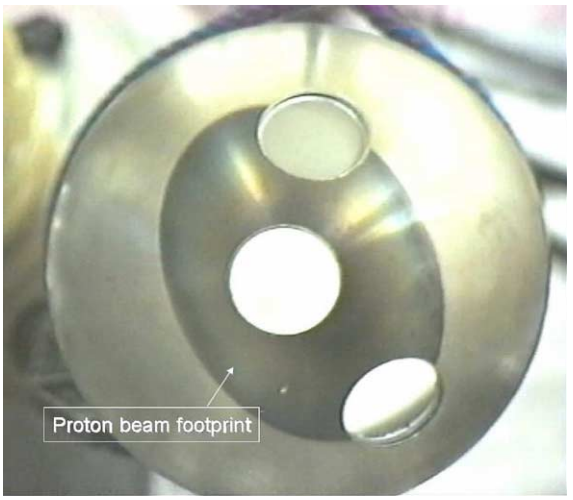

Fig. 2. A picture showing the beam window of the safety-hull of SINQ Target-3 after cutting discs (40 mm in diameter) at three positions.

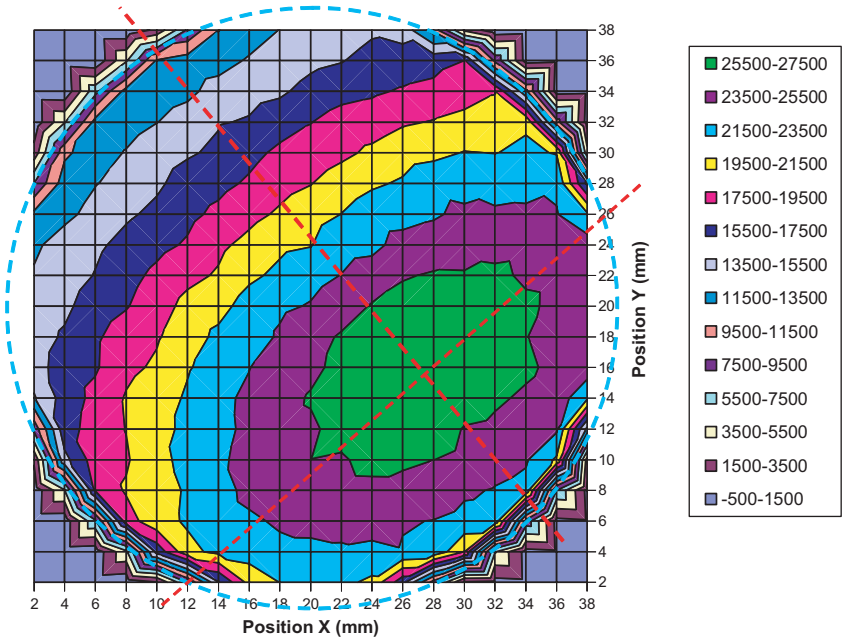

Fig. 3. γ-Mapping of Disc 1B from the center area (the middle hole shown in Fig. 2) of the beam window of the $AlMg_3$ safety-hull. The numbers are the counts of Na-22 measured in 20 min.

same way as the irradiated ones from an unirradiated safety-hull and four of them were tested together with the irradiated specimens. After tensile testing, the fracture surfaces of the specimens were observed with a scanning electron microscope (SEM) to identify the fracture mode.

The samples for microstructure study were cut from the grip sections of two irradiated tensile specimens of 0.7 and 3.6 dpa, and an unirradiated one. The microstructure was observed using a JEOL-2010 TEM and a Zeiss DSM932 SEM. The EDX analytical method on both TEM and SEM was also used to detect the changes in chemical composition.

3. Results

3.1. Tensile properties

The tensile test results are shown in Fig. 5. The four unirradiated specimens give a yield stress ($\sigma_{0.2}$) of 82 ± 5 MPa, an ultimate tensile strength of 203 ± 6 MPa, a

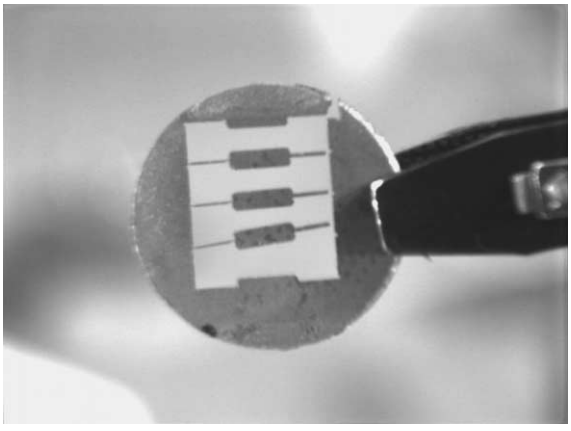

Fig. 4. A picture showing a disc after cutting four tensile specimens in a hot-cell.

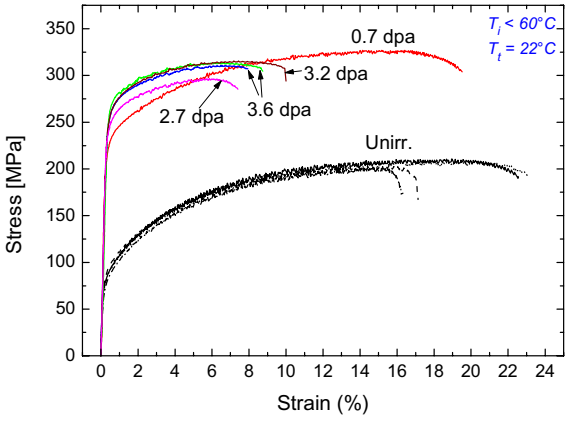

Fig. 5. Engineering stress–strain curves of the unirradiated and irradiated $AlMg_3$ specimens tested at room temperature.

uniform elongation of 17 ± 1.5% and a total elongation of 19 ± 3.5%. Both the yield stress and tensile strength increase significantly after irradiation. The ductility of the specimen of 0.7 dpa from the edge area of the proton beam remains, in fact, at the same level of the unirradiated ones, although its yield stress increases to about 230 MPa. For the specimens from the centre area, their uniform elongations drop to about 6.5% and the total elongations decrease to less than 9%.

The SEM observations on the fracture surfaces of the specimens demonstrate that they broke in a ductile mode, as shown in Fig. 6 for specimens of unirradiated, and irradiated to 0.7 and 3.6 dpa. However, comparing to that of the unirradiated specimen (Fig. 6(a) and (b)), the fracture surfaces of the irradiated specimens are slightly brittle (Fig. 6(c)–(f)) because they are flatter and less reduction in cross-section.

3.2. Precipitate structure

The precipitate structure in both irradiated and unirradiated material has been studied. In the present $AlMg_3$ alloy, precipitates can be distinguished according to their size: coarse ones, ~1 to few tens microns large, irregular in shape and mostly locating at grain boundaries (Fig. 7(a) and (b)); and fine ones, 10–500 nm large, plate-like and existing in the matrix (Fig. 7(c)). The composition of precipitates was analyzed with EDX device attached either with TEM or SEM. The results show that most of precipitates (Fig. 7(a) and (c)) are rich in Fe, Mn, Si and Al, while some relatively round ones are SiO_2 (Fig. 7(b)). It is also noted that the Si, Mn, and Fe contents vary greatly in different precipitates: 2–6 wt% for Si, 5–20 wt% for Mn and 5–20 wt% for Fe. The precipitates are partially amorphous after irradiation.

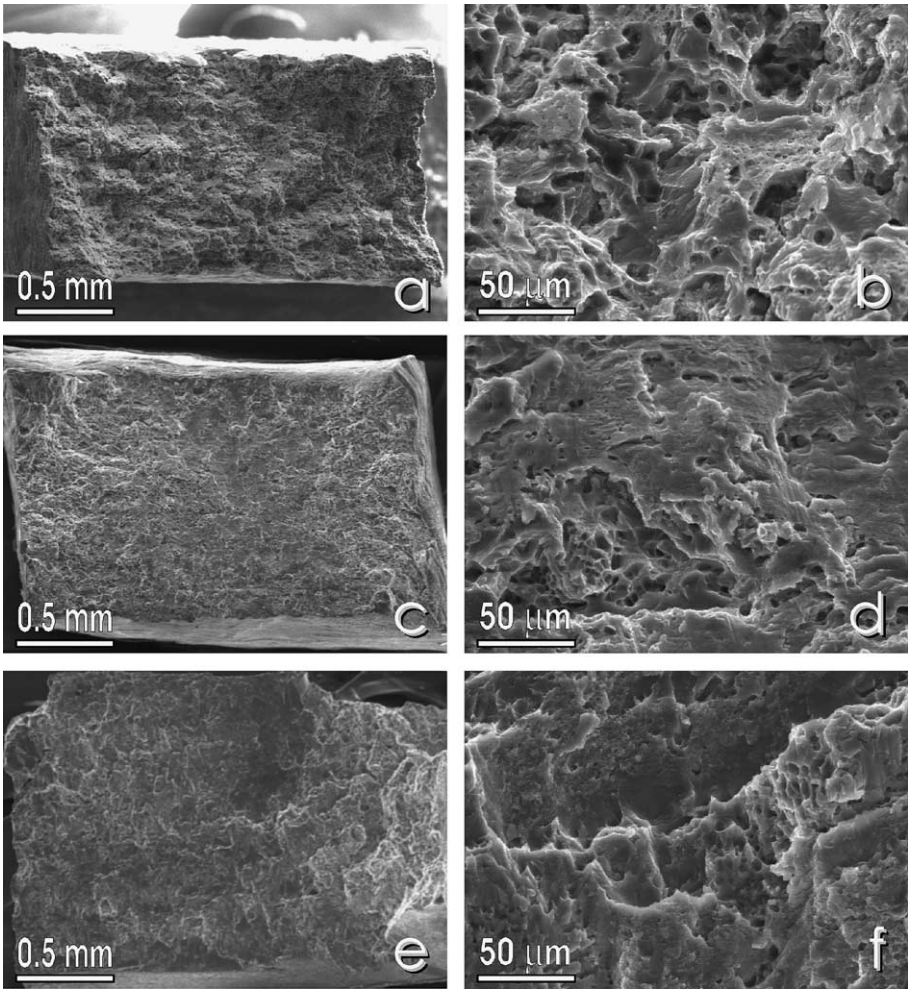

Fig. 6. SEM micrographs showing fracture surfaces of specimens in the unirradiated condition (a) and (b), and irradiated to 0.7 dpa (c) and (d) and 3.6 dpa (e) and (f).

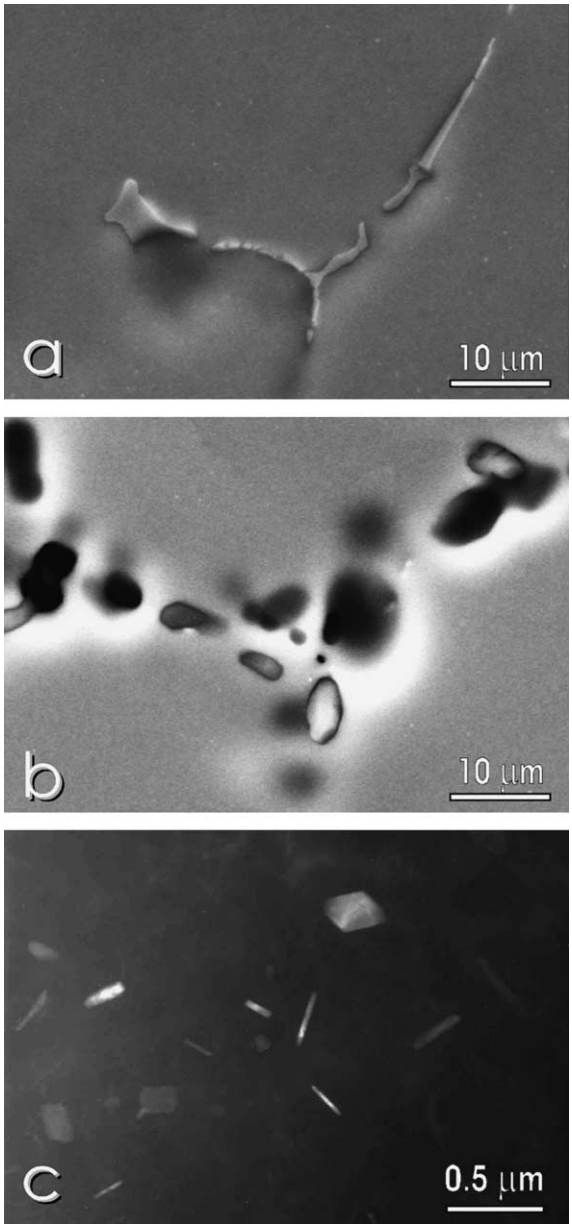

Fig. 7. SEM (a) and (b) and TEM (c) micrographs showing the morphology of precipitates in the $AlMg_3$ alloy.

3.3. Dislocation and helium bubble structures

The detailed description of the dislocation and helium bubble structures can be found in Ref. [2]. Here, only brief information will be described.

In the unirradiated material the dislocation density is not high. The dislocations are mainly located near small precipitates. In the irradiated samples of 0.7 and 3.6 dpa, high-density small dislocation loops and helium bubbles were observed, as shown in Fig. 8. The loop density does not change much with dose and is around $2.5 \times 10^{22}/m^3$, while the loop size increases significantly from about 6 nm at 0.7 dpa to about 14 nm at 3.6 dpa. The bubbles about 2 nm large distribute homogeneously in the matrix at 0.7 dpa. At 3.6 dpa, however, bubbles at grain boundaries are much larger than those in matrix. The size distribution of the bubbles in the matrix shows a bimodal manner. Most of the bubbles are similar to those in the 0.7 dpa sample, but the rest (~15%) of them are much larger (~5 nm). The large bubbles look preferentially locating along dislocation lines. The bubble density is about $1.5 \times 10^{23}/m^3$, which is more than 10 times higher than that in 0.7 dpa case, $1.2 \times 10^{22}/m^3$.

4. Discussion

Although some Al-alloys such as Al-6061 and Al-5052 have been well studied in both irradiated and unirradiated conditions, $AlMg_3$ alloy has been little studied even in the unirradiated condition. Nevertheless a study done by Lohmann and Singh et al. showed that the strength of the cold-worked $AlMg_3$ decreased drastically while the strength of the annealed material reduced only slightly after irradiated with 800 MeV protons to about 0.2 dpa at a temperature between 40 and 100 °C [6,7]. For the annealed specimen, no significant changes in the dislocation structure but an evident presence of helium bubbles at grain boundaries was observed after irradiation. The microstructure of the cold-worked specimen resembled closely the post-irradiation microstructure of the annealed specimen. Unfortunately, the irradiation dose of this study is much lower than the present ones and a direct comparison is not possible.

Generally, except for some precipitate hardened metals, irradiation hardening is observed at irradiation temperatures below about $0.35T_m$ (T_m is the absolute melting point temperature) due to the formation of small defect clusters or dislocation loops or precipitates induced by irradiation. In another Al-alloy, Al-5052 which has a chemical composition of 2.5% Mg and 0.25% Cr, Farrell observed a strong hardening after neutron irradiation [8,9]. In that case, the hardening was introduced by dislocation loops at lower doses and by the formation of small Mg_2Si precipitates at higher doses due to large amount of Si transformed via $^{27}Al(n,\gamma) \rightarrow {}^{28}Al \rightarrow {}^{28}Si + \beta$ reactions. In the present study, the irradiation dose is relatively low and the Si content is not so high. The observations here have some similarities to what was observed by Farrell at low doses (~2 dpa). For example, dislocation loops grew with increasing fluence, while no newly formed small Mg_2Si precipitates could be observed. However, in the present work, high-density small bubbles were observed, while Farrell observed only few cavities at a dose about 70 dpa. Although the composition difference of the two alloys may introduce

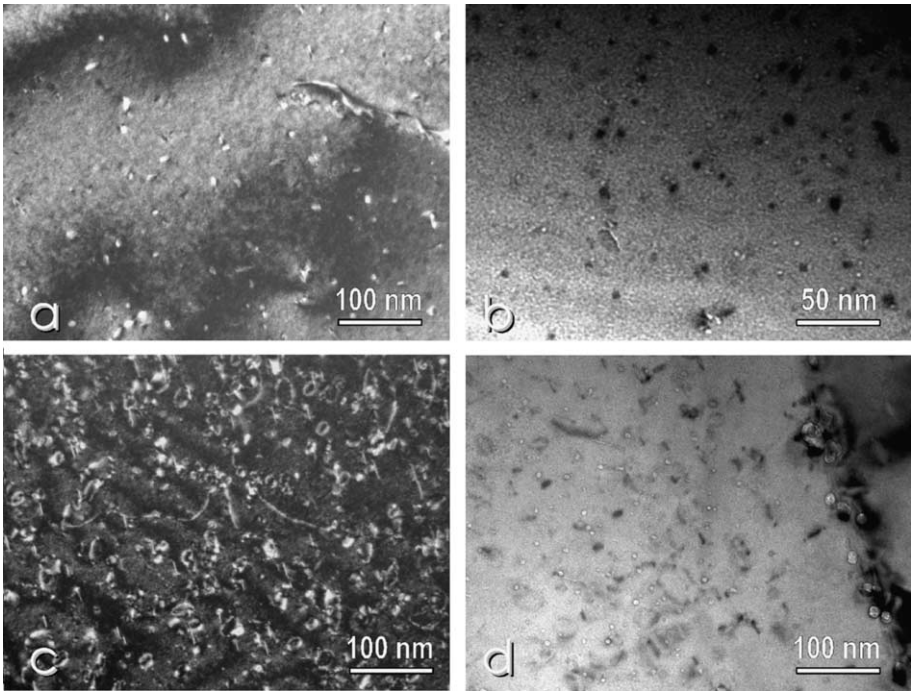

Fig. 8. TEM micrographs showing dislocation and helium bubble structures in the specimens of 0.7 dpa (a) and (b) and 3.6 dpa (c) and (d).

some difference in bubble formation which is strongly purity dependent for Al-alloys [9], the main reason for the formation of high-density small bubbles should be attributed to the high contents of helium and hydrogen produced by high energy protons.

The tensile properties of the unirradiated $AlMg_3$ are quite close to those of the unirradiated Al-5052, as shown in Fig. 9. However, it can be seen that the irradiation hardening (increase of yield stress and ultimate tensile strength) and embrittlement (decrease of uniform and total elongations) effects are much more pronounced in the present case as compared to the Al-5052 irradiated in the HFIR to similar doses, which is believed due to the presence of high-density helium bubbles. The in situ observations performed by Gavillet et al. on proton irradiated pure Al specimens demonstrated that small bubbles ($d \approx 7$ nm) are strong enough to stop dislocations, while larger bubbles ($d \geqslant 7$ nm) are weak obstacles to dislocation motion [10]. Almost all the bubbles observed in the grain interior are smaller than 7 nm. Therefore, a significant amount of hardening could be contributed by these small and dense bubbles. Of course, the density and size of the irradiation-induced dislocation loops in the $AlMg_3$ irradiated in the SINQ may be also different. But the comparison cannot be made since there is no data available for the Al-5052 irradiated in the HFIR. On the other hand, the drastic reduction in the uniform and total elongations of the $AlMg_3$ specimens at doses above about 2.7 dpa should be due to the high-density larger bubbles at grain boundaries, although no typical intergranular fracture was observed on the fracture surfaces.

Hence, it can be concluded that high energy proton irradiation produce more drastic degradation of the mechanical properties of aluminum alloys than fission neutron irradiation. Whether the embrittlement effects will saturate at higher doses will be studied in the future on the same material irradiated in the followed SINQ targets.

5. Conclusions

In the present study, $AlMg_3$ alloy was irradiated in SINQ Target-3 at $\leqslant 60$ °C to doses up to 3.6 dpa with helium contents up to 1100 appm. Tensile tests, SEM and TEM observations have been performed and the results demonstrate:

(1) The irradiation induced significant hardening and embrittlement: the yield stress and tensile strength increased while the ductility decreased substantially after irradiation. However fracture of the specimens is still in a ductile mode.

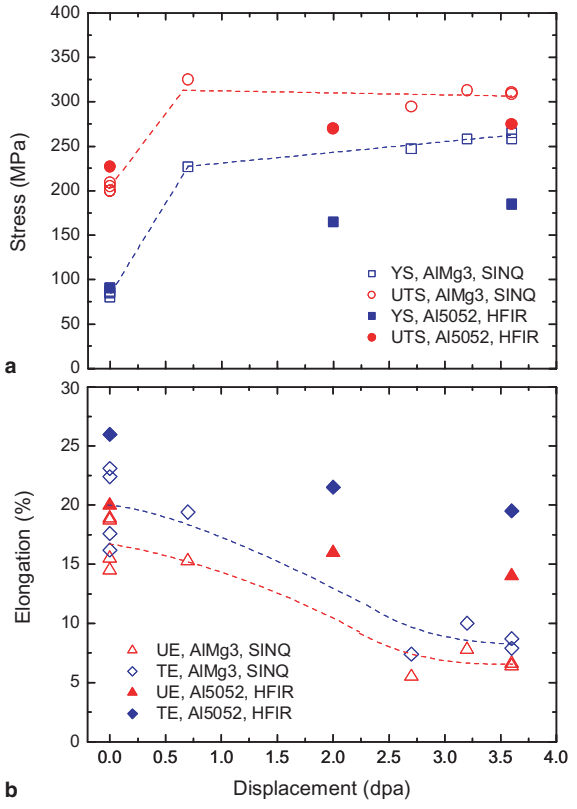

Fig. 9. The irradiation dose dependence of (a) yield stress (YS) and ultimate tensile strength (UTS), (b) uniform elongation (UE) and total elongation (TE). For a comparison, a few data of Al-5052 irradiated in the HFIR [8] were included.

(2) The TEM observations show that the irradiation produced high-density dislocation loops and helium bubbles. The bubbles locate preferentially at dislocations and grain boundaries. The bubbles at grain boundaries are much larger than those in gain interior.
(3) The presence of high-density bubbles may greatly enhance both irradiation hardening and embrittlement effects.

References

[1] Y. Dai, G.S. Bauer, J. Nucl. Mater. 296 (2001) 43.
[2] D. Hamaguchi, Y. Dai, J. Nucl. Mater. 329–333 (2004) 958.
[3] L.P. Ni, Presentation at the 1st MEGAPIE Technical Review Meeting, Cadarache, France, 2001.
[4] W. Lu, M.S. Wechsler, Y. Dai, J. Nucl. Mater. 318 (2003) 176.
[5] Y. Dai, Y. Foucher, M.R. James, B.M. Oliver, J. Nucl. Mater. 318 (2003) 167.
[6] W. Lohmann, A. Ribbens, W.F. Sommer, B.N. Singh, Radiat. Eff. 101 (1987) 283.
[7] B.N. Singh, W. Lohmann, A. Ribbens, W.F. Sommer, in: Radiation-induced Changes in Microstructure, ASTM STP 955, 1987, p. 508.
[8] K. Farrell, J. Nucl. Mater. 97 (1981) 33.
[9] K. Farrell, in: Dimensional Stability and Mechanical Behaviour of Irradiated Metals and Alloys, British Nuclear Energy Society, London, 1983, p. 72.
[10] D. Gavillet, W.V. Green, M. Victoria, R. Gotthardt, J.L. Martin, in: Radiation-induced Changes in Microstructure, ASTM STP 955, 1987, p. 490.